J Mater Sci (2007) 42:2574–2581
DOI 10.1007/s10853-006-1294-y

Correlation between interfacial microstructure and shear behavior of Sn–Ag–Cu solder ball joined with Sn–Zn–Bi paste

Po-Cheng Shih · Kwang-Lung Lin

Received: 24 June 2005 / Accepted: 30 January 2006 / Published online: 2 January 2007

Abstract Sn–8Zn–3Bi solder paste was applied as a medium to joint Sn–3.2Ag–0.5Cu solder balls and Cu/Ni/Au metallized ball grid array substrates at 210 °C. Sn–Ag–Cu joints without Sn–Zn–Bi addition were also conducted for comparison. The shear behavior of the specimens was investigated after multiple reflow and thermal aging. For each strength test, more than 40 solder balls were sheared. The shear strength of Sn–Ag–Cu specimens kept constant ranging from 15.5 ± 1.3 N (single reflow) to 16.2 ± 1.0 N (ten reflows) and the fractures occurred in the solder. Shear strength of Sn–Ag–Cu/Sn–Zn–Bi specimens fell from 15.9 ± 1.7 N (single reflow) to 13.4 ± 1.6 N (ten reflows). After single reflow, Sn–Ag–Cu/Sn–Zn–Bi specimens fractured in the solder along Ag–Au–Cu–Zn intermetallic compounds and at Ni metallization. After ten reflows, fractures occurred in the solder and at solder/Ni–Sn–Cu–Zn intermetallic compound interface. The shear strengths of the Sn–Ag–Cu and Sn–Ag–Cu/Sn–Zn–Bi packages changed little after aging at 150 °C. Sn–Ag–Cu/Sn–Zn–Bi joints kept higher strength than Sn–Ag–Cu joints. Sn–Ag–Cu joints fractured in the solder after aging. But the fractures of Sn–Ag–Cu/Sn–Zn–Bi specimens shifted to the solder with aging time.

P.-C. Shih (✉) · K.-L. Lin
Department of Materials Science and Engineering, National Cheng-Kung University, No.1, Ta-Hsueh Road, Tainan 701, Taiwan, R.O.C.
e-mail: pj.shih@msa.hinet.net

Introduction

Sn–Pb solder balls have been used to joint the Ball Grid Array (BGA) packages to Printed Circuit Boards (PCBs) due to low eutectic melting temperature (around 183 °C) and good wetting behavior on several substrate metallizations such as Cu, Ag, Pd and Au [1–3]. However, lead (Pb) is toxic and detrimental to the environment and our health. Hence the legislative ban on the use of Pb-based solders is driving the need for the Sn–Pb solder substitute. A number of Pb-free solders have been proposed. Among these, Sn/Ag-based alloys hold promise because of their good resistance to thermal fatigue, high ductility [4] and better solderability on copper than Sn–Pb solder [5]. Investigations have been conducted to modify the thermal and mechanical characteristics of eutectic Sn–3.5Ag solder with the addition of Bi, Cu, In, Sb or Zn [6–11]. Additions in Sn–Ag eutectic solder not only decrease the melting point but also enhance mechanical properties.

Sn–Zn solder (Sn–9mass% Zn for the eutectic composition), with a eutectic temperature of 199 °C, has also been investigated as a lead-free solder. Moreover, the addition of Bi to Sn–Zn near eutectic solder can improve the soldering properties by lowering melting temperature to 188–199 °C [3, 4].

In spite of the compositional modification, the melting points of the Sn–Ag- or Sn–Zn-based solders are still 15–60 °C higher than that of the Sn–Pb eutectic solder. This is expected to result in the excessive growth of intermetallic compounds (IMCs) during the soldering process [12]. The overgrown IMCs are detrimental to the bonding strength between the solder and the substrate due to increased brittleness

[13]. To overcome this problem, the Sn–Zn–Bi solder paste of lower melting temperature (roughly 188–199 °C) may apply in Sn–Ag–Cu packages as a joint medium between the Sn–Ag–Cu solder ball and the metallization pad during soldering.

The soldering temperature of Sn–Ag–Cu packages may be lowered with the introduction of Sn–Zn–Bi paste to inhibit the excessive growth of intermetallic compounds. The purpose of this study was to investigate the correlation between interfacial microstructures and shear properties of the Sn–Ag–Cu packages which apply the Sn–Zn–Bi solder paste. Moreover, the shear property of Sn–Ag–Cu packages without Sn–Zn–Bi addition is compared.

Experimental procedure

Commercial Sn–8Zn–3Bi solder paste and Sn–3.2Ag–0.5Cu (mass %) solder balls were used in this study. The solder paste was composed of activated flux and Sn–Zn–Bi solder particles (20–25 μm in diameter). The solder balls were 760 μm in diameter. Prior to the soldering process, the solder paste with a thickness of 200 μm was stencil printed onto Cu/Ni/Au-metallized pad on the commercial BGA substrate, followed by solder ball attachment on the paste-covered pad, as shown in Fig. 1. The copper layer was 30 μm in thickness, and the thicknesses of the nickel and gold layers were 7 μm and 1 μm, respectively. In addition to the Sn–Ag–Cu/Sn–Zn–Bi joints, the Sn–Ag–Cu joints without paste were studied for comparison.

Shear test was conducted for multiple reflowed and thermally aged BGA specimens. Multiple reflow were conducted for 1, 5, and 10 cycles. The thermal aging

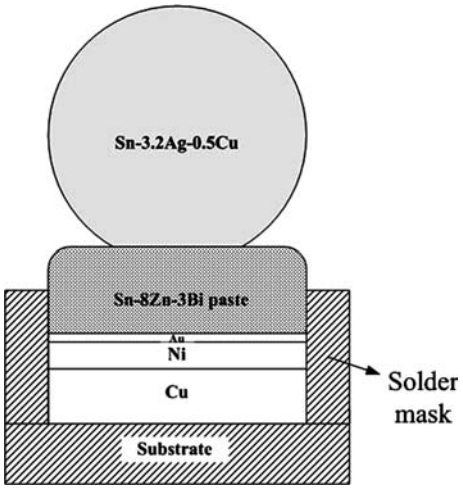

Fig. 1 Cross-sectional sketch of the Sn–Ag–Cu/Sn–Zn–Bi joint before reflow

was conducted at 150 °C after single reflow cycle for 100, 200, 500 and 1,000 h. The reflow experiment was performed in an infrared (IR) furnace under a protective atmosphere of 90%N_2–10%H_2. The reflow profile consisted of an activation stage at 170 °C with a peak temperature of 210 °C (for Sn–Ag–Cu/Sn–Zn–Bi samples) or 240 °C (for Sn–Ag–Cu samples) for 30 s and then a descent to room temperature over 3–4 min. The ball shear test was conducted at a constant shear speed of 0.5 mm/s with a fixed shear tip height of 50 μm above the BGA substrate. The fracture surface and microstructure of the BGA joints were polished with 0.3-μm Al_2O_3 powder, and investigated by scanning electron microscope (SEM), and energy dispersive X-ray analysis (EDX).

Experimental results

Microstructure of the samples

Sn–Ag–Cu system

Figure 2a shows the SEM micrographs of both the solder bulk and the interface between Sn–Ag–Cu solder and Cu/Ni BGA substrate after single reflow. During reflow soldering, the topmost Au layer dissolves into the molten solder, leaving the Ni layer exposed to the molten solder. According to the EDX results, the interfacial reaction between molten solder and the Ni layer results in the formation of the pyramid-shaped compound (Cu:Ni Sn = 39:17:44, at %) and layered compound (Ni:Cu:Sn = 36:7:57, at %) of 1.2 μm thick, which respectively imply (Cu, Ni)$_6$Sn$_5$ and (Ni, Cu)$_3$Sn$_4$ by atomic ratio [5, 14–17], as shown in Fig. 2a. The microstructure of the bulk material indicates the darker regions of Sn-rich areas, which are surrounded by brighter particle-sized Ag_3Sn intermetallic compounds [5, 14, 15]. After ten reflows (Fig. 2b), the interfacial (Ni, Cu)$_3$Sn$_4$ grows further toward 3–4 μm thick. Two grown (Cu, Ni)$_6$Sn$_5$ grains tend to incorporate to lower the surface energy. After aging for 1,000 h (Fig. 2c), the compounds of (Cu, Ni)$_6$Sn$_5$, (Ni, Cu)$_3$Sn$_4$ and Ag_3Sn do not show the significant grain growth.

Sn–Ag–Cu/Sn–Zn–Bi system

Figure 3a shows the SEM micrograph of Sn–Ag–Cu/Sn–Zn–Bi solder jointed with Cu/Ni/Au BGA substrate after single reflow cycle. The Ni–Sn–Cu–Zn compound with a thickness of 1 μm forms at the interface of which atomic ratio is Ni:Sn:Cu:Zn = 27:43:13:16 (at %), mainly

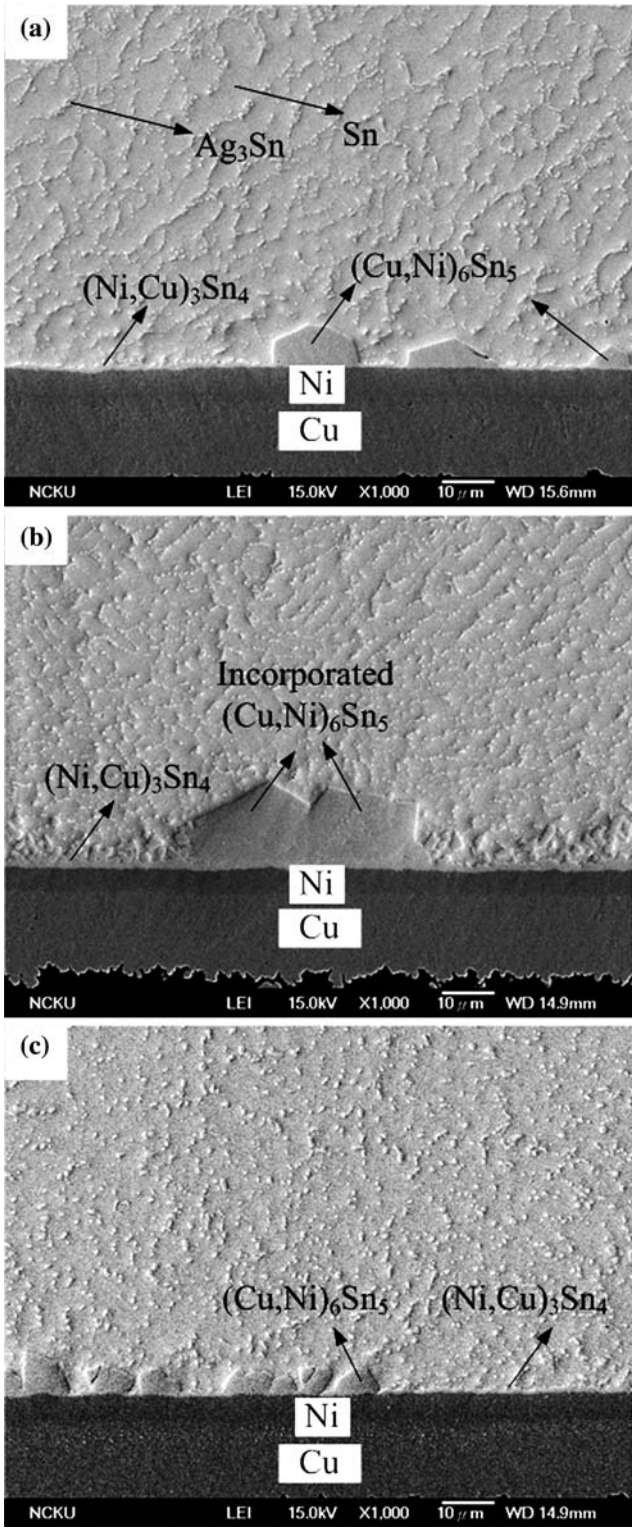

Fig. 2 Interfacial microstructures of the Sn–Ag–Cu specimens after (**a**) single reflow, (**b**) ten reflows and (**c**) aging for 1,000 h

consisting of Ni and Sn. According to Ag–Zn and Ag–Sn phase diagrams [18, 19], the compounds identified in the solder are likely to be Ag_5Zn_8 (Ag:Zn = 41:59, at %) and Ag_3Sn (Ag:Sn = 74:26, at %). Moreover, the layered Ag–Au–Cu–Zn compound detaches from the interface and moves into the solder after single reflow. Elemental compositions of Ag, Au and Cu distribute in Ag–Au–Cu–Zn compounds of which atomic ratios of points A and B are respectively Ag:Au:Cu:Zn = 10:7:20:63 and 7:17:12:64 (at %). Bi is not identified in any compounds. According to Bi–Sn phase diagram [20], Bi may dissolve in Sn phase due to notable solubility from 5 (50 °C) to 21 at % (140 °C). Figure 3b, c indicates that micro-cracks are identified locally between Ag–Au–Cu–Zn IMCs and Ni metallization after single reflow. Figure 4a and 4b, c respectively show SEM micrographs of Sn–Ag–Cu/Sn–Zn–Bi solder jointed with Cu/Ni BGA substrate after five and ten reflows. Ni–Sn–Cu–Zn IMCs grow significantly from 3.2 μm thick (five cycles) to 5.0 μm (ten cycles). Ag–Au–Cu–Zn IMC layer appears to shrink with reflow cycles (Fig. 4b), or even shrinks to disappear (Fig. 4c). The reason of Ag–Au–Cu–Zn IMC shrinkage is not clear and needs further study.

Figure 5a–c respectively show SEM micrographs of Sn–Ag–Cu/Sn-Zn-Bi solder jointed with Cu/Ni/Au substrate after aging for 200, 500 and 1,000 h. Solid-state aging at 150 °C results in the growth of Ni–Sn–Cu–Zn compounds from 1 μm (single reflow, or aging 0 h) to 2.1 μm thick (aging 1,000 h), as shown in Figs. 3a and 5c. Ag_3Sn is embedded in Ni–Sn–Cu–Zn IMCs. Layered Ag–Au–Cu–Zn IMCs appear not to thicken with aging time.

The shear behaviors of the samples

Figure 6a, b respectively shows the effects of reflow cycle and aging time on shear strength. Figure 6a shows that the shear strength of Sn–Ag–Cu joints (labeled SAC) deviates slightly from single reflow (15.5 ± 1.3 N) to ten reflows (16.2 ± 1.0 N). However, the shear strength of Sn–Ag–Cu/Sn–Zn–Bi joints (labeled SAC + SZB) falls from single reflow (15.9 ± 1.7 N) to five reflows (13.8 ± 1.4 N) and changes little from 5 to 10 reflows (13.4 ± 1.6 N). After thermal aging for 1,000 h, the adhesion strengths of both joint systems change little, as shown in Fig. 6b. The strengths of Sn–Ag–Cu joints are 15.0 ± 1.4 N, 15.8 ± 1.1 N, 15.3 ± 1.1 N and 15.2 ± 1.3 N and those of Sn–Ag–Cu/Sn–Zn–Bi joints are 15.6 ± 1.2 N, 16.5 ± 1.4 N, 16.7 ± 1.5 N and 16 ± 1.3 N after aging for 100, 200, 500 and 1,000 h, respectively. It is noted that Sn–Ag–Cu/Sn–Zn–Bi joints hold higher strength than Sn–Ag–Cu joints.

Figure 7a–c shows that the Sn–Ag–Cu joints fracture in the solder after single reflow (7a), ten reflows (7b) and aging for 1,000 h (7c). Figure 8a–e shows the cross-sectional morphology of the Sn–Ag–Cu/Sn–Zn–Bi sheared specimens after various reflows. Figure 8b, c

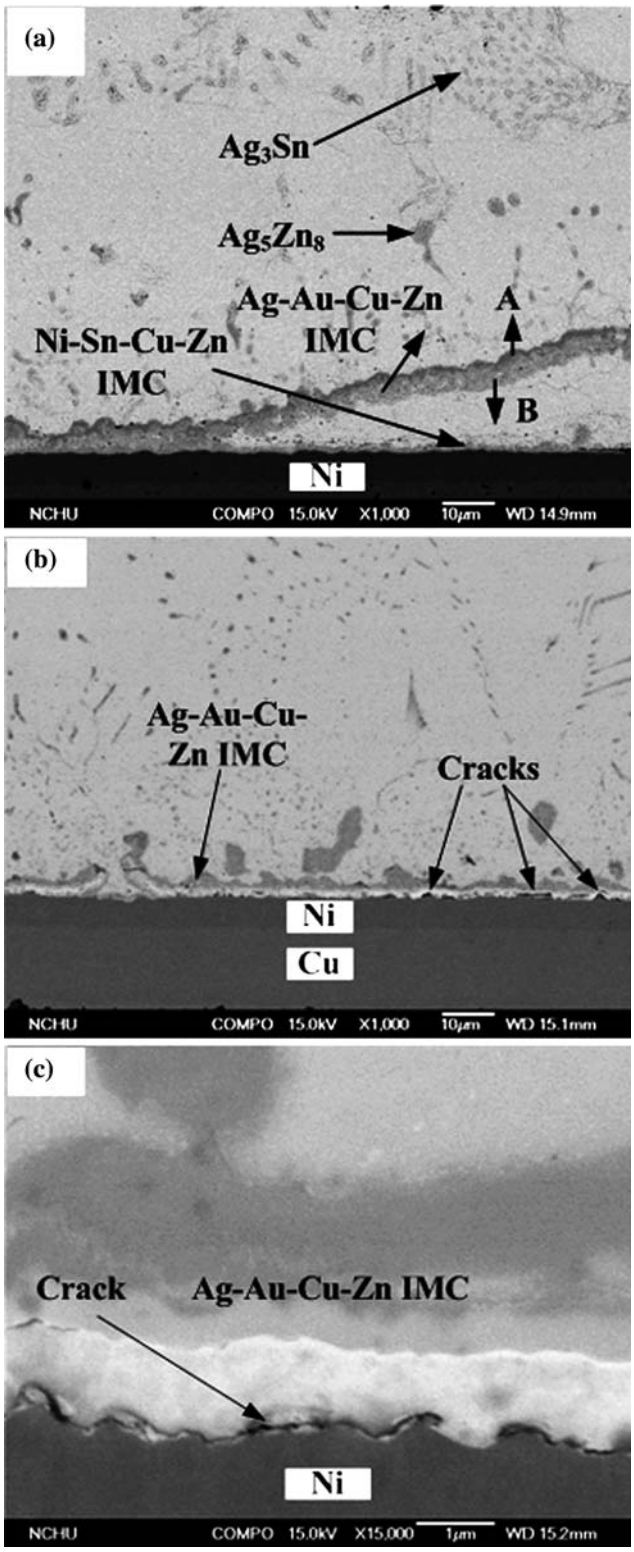

Fig. 3 Interfacial microstructures of the Sn–Ag–Cu/Sn–Zn–Bi specimens after single reflow: (**a**) IMC observation in the solder and interfacial area, (**b**) local crack formation and (**c**) magnification image of the crack between Ag–Au–Cu–Zn IMC and Ni metallization

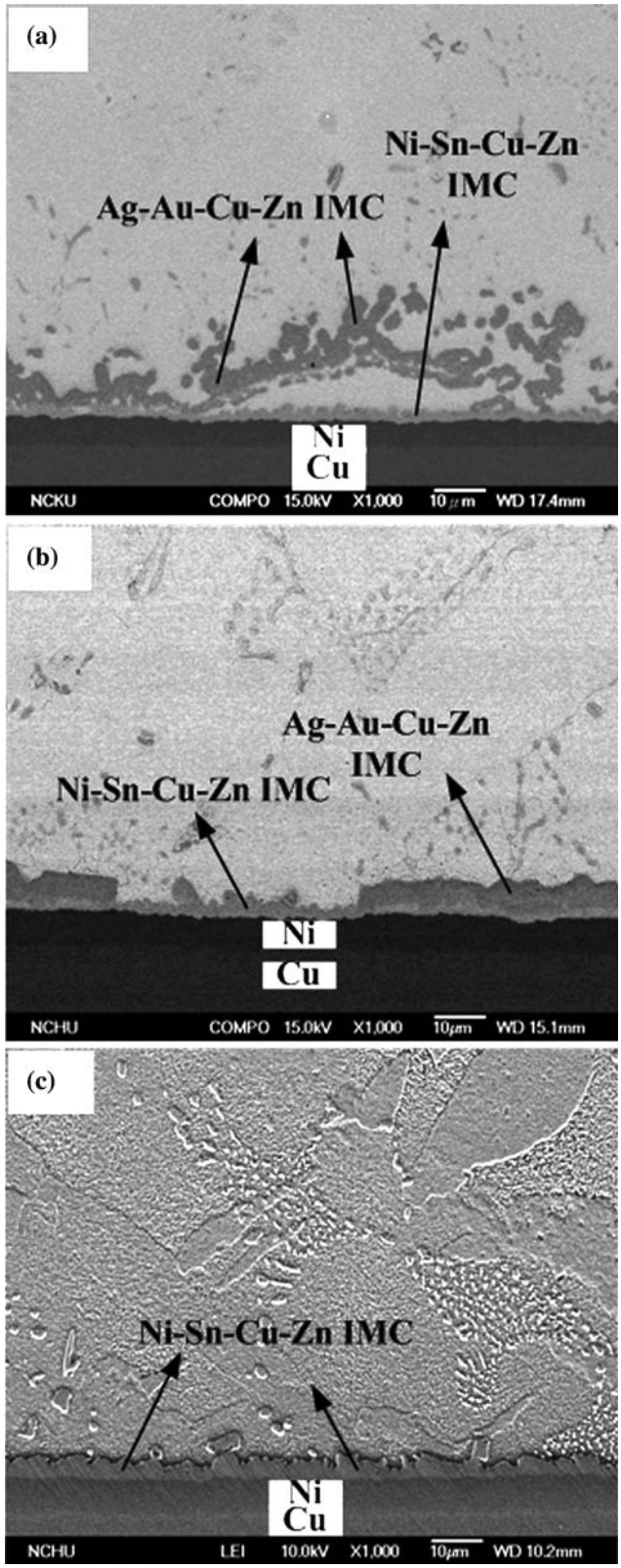

Fig. 4 Interfacial microstructures of the Sn–Ag–Cu/Sn–Zn–Bi specimens after (**a**) five reflows and (**b, c**) ten reflows

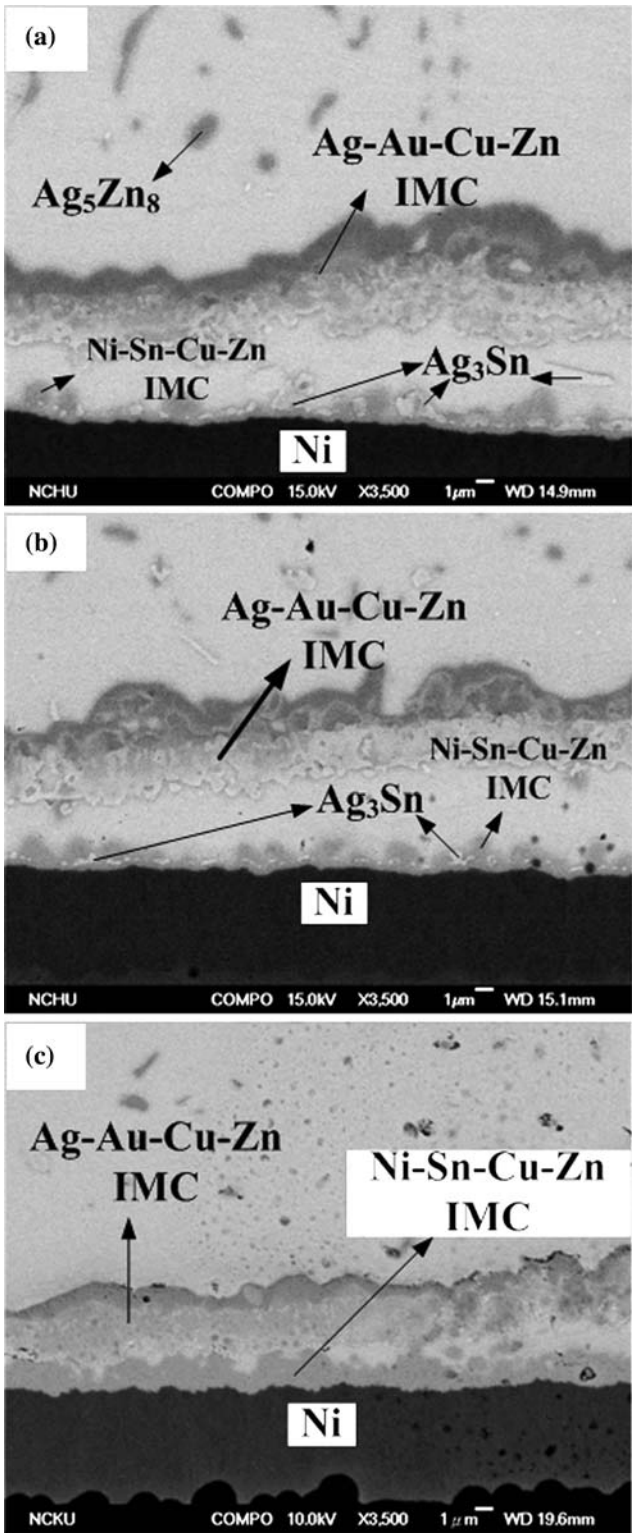

Fig. 5 Interfacial microstructures of the Sn–Ag–Cu/Sn–Zn–Bi specimens aged for (**a**) 200 h, (**b**) 500 h and (**c**) 1,000 h

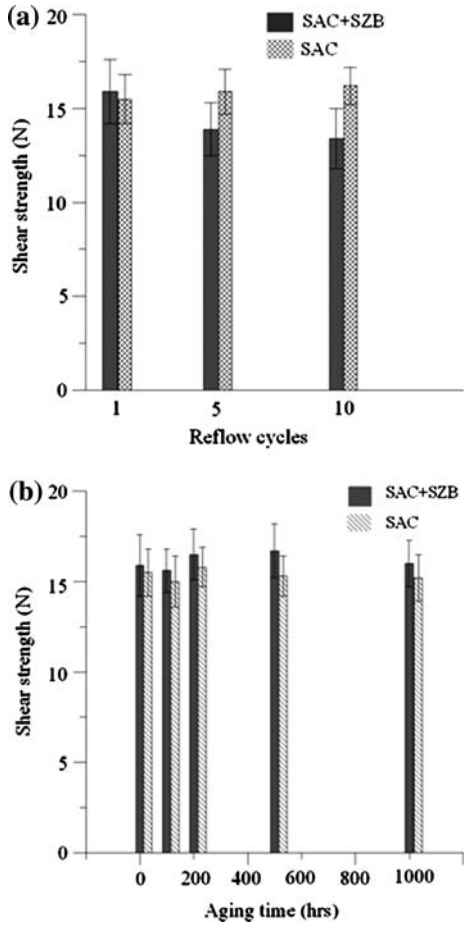

Fig. 6 Shear strength variation by (**a**) multiple reflows and (**b**) thermal aging treatment (SAC: Sn–Ag–Cu joints, SAC+SZB: Sn–Ag–Cu/Sn–Zn–Bi joints)

(magnifications of Regions A and B in Fig. 8a) shows that, after single reflow, the fractures occurred in the solder along Ag–Au–Cu–Zn IMCs (Fig. 8b) and at Ni metallization (Fig. 8c). After five reflows (Fig. 8d), fracture occurs in the solder along Ag–Au–Cu–Zn IMCs and at solder/Ni–Sn–Cu–Zn IMC interface. After ten reflows, shrinking Ag–Au–Cu–Zn IMCs are hardly observed in the sheared solder. The fracture occurs in the solder and at solder/Ni–Sn–Cu–Zn IMC interface (Fig. 8e).

Figure 9a–d shows the cross-sectional morphology of the Sn–Ag–Cu/Sn–Zn–Bi sheared specimens aged for different time. Fractures occur in the solder along Ag–Au–Cu–Zn IMCs and at Ni metallization after aging for 100 (Fig. 9a) and 200 h (Fig. 9b). However, fractures gradually shift to the solder as aging time increases from 500 (Fig. 9c) to 1,000 h (Fig. 9d).

Discussion

For Sn–Ag–Cu joints, fractures occurring in the solder indicate that the interfacial compounds are minor to failure behavior. Moreover, the microstructure of the

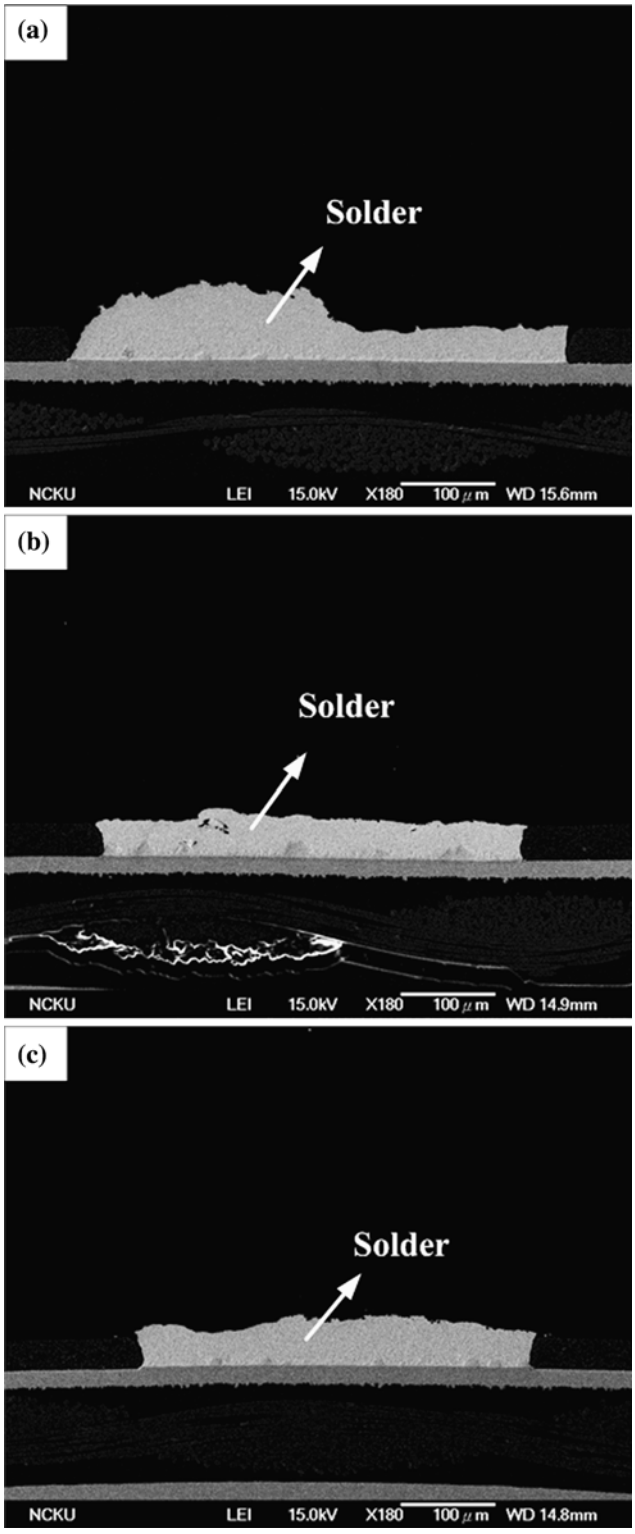

Fig. 7 Cross-sectional fractures of the Sn–Ag–Cu joints after (**a**) single reflow, (**b**) ten reflows and (**c**) aging for 1,000 h

bulk seems not to change significantly with reflows or aging time, which may result in the constant shear strength.

For Sn–Ag–Cu/Sn–Zn–Bi joints, the fracture occurring in the solder along the Ag–Au–Cu–Zn compounds may be ascribed to the detachment of Ag–Au–Cu–Zn compounds into the solder which deteriorates the joint strength due to IMC brittleness. Furthermore, the fracture occurred at Ni metallization is likely due to the crack formation (Fig. 3b, c) between Ag–Au–Cu–Zn compounds and Ni metallization. The reason for crack formation is not clear and the related studies are in progress. After five reflows, interfacial Ni–Sn–Cu–Zn IMCs grow to provide the significant joint strength with Ni metallization. But the grown Ni–Sn–Cu–Zn IMCs may degrade the joint strength between the brittle Ni–Sn–Cu–Zn IMCs and the ductile solder, contributing to the drops of the strength from 1 to 5 reflow cycles. The constant shear curve from 5 to 10 reflows may be ascribed to the similar fractures (at solder/Ni–Sn–Cu–Zn compound interface). It implies that the thickness of Ni–Sn–Cu–Zn compounds may not involve in altering the joint strengths but adhere notably with Ni metallization. After ten reflows, the effect of the shrinkage of Ag–Au–Cu–Zn IMCs on bonding strength is possibly insignificantly in that they are hardly found in fractures. As aging test proceeds, the growing Ni–Sn–Cu–Zn compounds also provide a significant bonding with Ni metallization and result in the transformation of the shear fracture to solder with aging time toward 1,000 h. It suggests that the bonding strength between thickened layered Ni–Sn–Cu–Zn compounds and Ni metallization seems to be higher than that of the solder, leading to the fractures in the solder instead of at Ni metallization. Nevertheless, the shear strength curve shown in Fig. 6b does not exhibit the behavior. This is because the fractures usually occur in the region of lower shear strength (the solder, in this study), not in higher strength region (at Ni metallization). Hence it is unable to measure the strength between thickened layered Ni–Sn–Cu–Zn compounds and Ni metallization. As mentioned above, it is noted that Sn–Ag–Cu/Sn–Zn–Bi joints keep higher strength than Sn–Ag–Cu joints in each corresponding aging test. This phenomenon may be due to the Bi addition because Bi is generally considered to be hard which causes solid solution hardening of the Sn phase [6, 21–23].

Soldering at lower temperature is beneficial for energy saving and the inhibition of excessive IMC growth. However, it may cause the poor bonding strength between solder and metallization pad due to the deficient interfacial reaction. Although Sn–Ag–Cu/Sn–Zn–Bi joints hold lower strengths than Sn–Ag–Cu joints under multiple reflows, thus produced packages (Sn–Ag–Cu/Sn–Zn–Bi joints) also meet the minimum

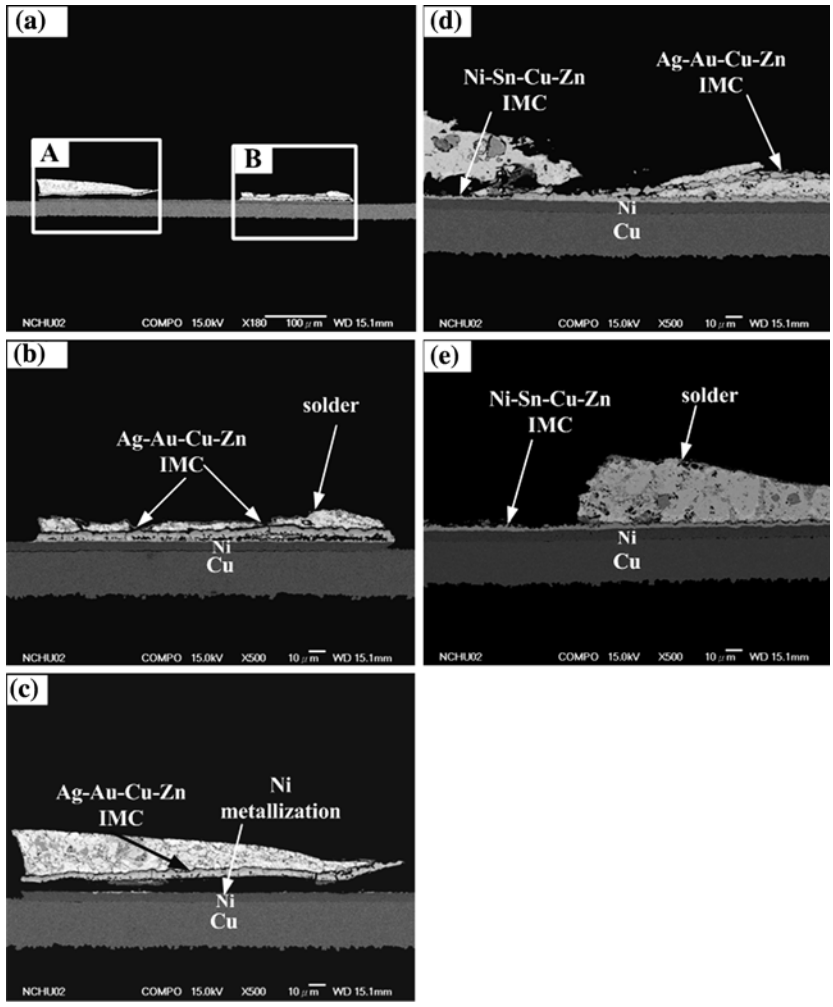

Fig. 8 Cross-sectional fractures of the Sn–Ag–Cu/Sn–Zn–Bi joints after various reflows: (**a**) single reflow, (**b**) the magnification of Region A in (**a**), (**c**) the magnification of Region B in (**a**), (**d**) five reflows and (**e**) ten reflows

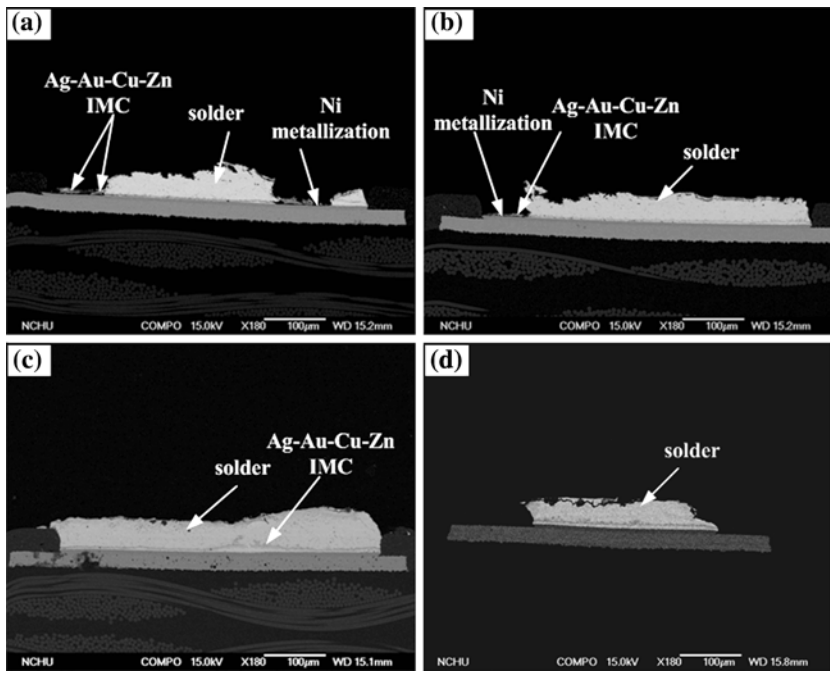

Fig. 9 Cross-sectional fractures of the Sn–Ag–Cu/Sn–Zn–Bi joints after aging for: (**a**) 100 h, (**b**) 200 h, (**c**) 500 h and (**d**) 1,000 h

ball shear force of 1 kg (9.8 N) in the industry benchmark test [24]. As a result, the introduction of Sn–Zn–Bi medium to join the Sn–Ag–Cu solder ball with metallization pads seems to preserve the notable bonding strength of BGA packages, even at a low soldering temperature of 210 °C. However, it still needs further reliability tests for practical feasibility purpose.

Conclusion

The soldering temperature of Sn–3.2Ag–0.5Cu BGA packages were successfully lowered to 210 °C with the introduction of Sn–8Zn–3Bi solder paste as a joint medium. Sn–Ag–Cu joints without Sn–Zn–Bi addition were also conducted for comparison. The shear strength of Sn–Ag–Cu specimens kept constant ranging from 15.5 ± 1.3 N (single reflow) to 16.2 ± 1.0 N (ten reflows) and the fractures occurred in the solder. Shear strength of Sn–Ag–Cu/Sn–Zn–Bi specimens fell from 15.9 ± 1.7 N (single reflow) to 13.4 ± 1.6 N (ten reflows). After single reflow, Sn–Ag–Cu/Sn–Zn–Bi specimens fractured in the solder along Ag–Au–Cu–Zn IMCs and at Ni metallization. After ten reflows, fractures occurred in the solder and at solder/Ni–Sn–Cu–Zn IMC interface. The shear strengths of the Sn–Ag–Cu and Sn–Ag–Cu/Sn–Zn–Bi packages changed little after aging at 150 °C. Sn–Ag–Cu/Sn–Zn–Bi joints kept higher strength than Sn–Ag–Cu joints. Sn–Ag–Cu joints fractured in the solder after aging. Nevertheless, the fractures of Sn–Ag–Cu/Sn–Zn–Bi specimens shifted to the solder with aging time.

Acknowledgements Financial support for this work provided by the National Science Council of R.O.C. (Taiwan) under grant NSC91-2216-E-006-035 is gratefully acknowledged. The authors also thank Accurus Scientific Co., LTD. for supplying the solder balls.

References

1. Amagai M, Watanabe M, Omiya M, Kishimoto K, Shibuya T (2002) Microelectron Reliab 42:951
2. Hirose A, Fujii T, Imamura T, Kobayashi KF (2001) Mater Trans 42(5):794
3. Miyazawa Y, Ariga T (2001) Mater Trans 42(5):776
4. Chonan Y, Komiyama T, Onuki J, Urao R, Kimura T, Nagano T (2002) Mater Trans 43(8):1887
5. Chuang CM, Shih PC, Lin KL (2004) J Electron Mater 33(1):1
6. Choi JW, Cha HS, Oh TS (2002) Mater Trans 43(8):1864
7. Jang JW, Frear DR, Lee TY, Tu KN (2000) J Appl Phys 88(11):6359
8. Bradley E III, Hranisavljevic J (2000). In: Electronic components and technology conference, 2000 proceedings 50th, 21–24 May 2000, p 1443
9. Vianco PT, Rejent JA (1999) J Electron Mater 28(11):1127
10. Vianco PT, Rejent JA (1999) J Electron Mater 28(11):1138
11. Kariya Y, Otsuka M (1998) J Electron Mater 27(7):866
12. Kang SK, Choi WK, Shih DY, Lauro P, Henderson DW, Gosselin T, Leonard DN (2002) In: Electronic components and technology conference, 2002 proceedings 52nd, 28–31 May 2002, p 146
13. Lee CB, Jung SB, Shin YE, Shur CC (2002) Mater Trans 43(8):1858
14. Kim SW, Yoon JW, Jung SB (2004) J Electron Mater 33(10):1182
15. Ghosh G (2004) J Electron Mater 33(10):1080
16. Lin YL, Luo WC, Lin YH, Ho CE, Kao CR (2004) J Electron Mater 33(10):1092
17. Jang GY, Huang CS, Hsiao LY, Duh JG, Takahashi H (2004) J Electron Mater 33(10):1118
18. Massalski TB (1986) Binary alloy phase diagrams, vol. 1. ASM, Metals Park, Ohio, USA, pp 85–86
19. Massalski TB (1986) Binary alloy phase diagrams, vol. 1. ASM, Metals Park, Ohio, USA, pp 69–71
20. Massalski TB (1986) Binary alloy phase diagrams, vol. 1. ASM, Metals Park, Ohio, USA, pp 540–541
21. Nishiura M, Nakayama A, Sakatani S, Kohara Y, Uenishi K, Kobayashi KF (2002) Mater Trans 43(8):1802
22. Shimokawa H, Soga T, Serizawa K (2002) Mater Trans 43(8):1808
23. Islam RA, Wu BY, Alam MO, Chan YC, Jillek W (2005) J Alloys Comp 392:149
24. Coyle RJ, Solan PP, Serafino AJ, Gahr SA (2000) In: electronic components and technology conference, 2000 proceedings 50th, 21–24 May 2000, p 160